JACS
JOURNAL OF THE AMERICAN CHEMICAL SOCIETY
Communication
pubs.acs.org/JACS

A Robust Binary Supramolecular Organic Framework (SOF) with High CO_2 Adsorption and Selectivity

Jian Lü,[†,‡] Cristina Perez-Krap,[†] Mikhail Suyetin,[†] Nada H. Alsmail,[†] Yong Yan,[†] Sihai Yang,[†] William Lewis,[†] Elena Bichoutskaia,[†] Chiu C. Tang,[§] Alexander J. Blake,[†] Rong Cao,[‡] and Martin Schröder*[,†]

[†]School of Chemistry, University of Nottingham, Nottingham NG7 2RD, United Kingdom

[‡]State Key Laboratory of Structural Chemistry, Fujian Institute of Research on the Structure of Matter, Chinese Academy of Sciences, Fujian Fuzhou 350002, P. R. China

[§]Diamond Light Source, Harwell Science and Innovation Campus, Didcot, Oxfordshire, OX11 0DE, United Kingdom

Supporting Information

ABSTRACT: A robust binary hydrogen-bonded supramolecular organic framework (**SOF-7**) has been synthesized by solvothermal reaction of 1,4-bis-(4-(3,5-dicyano-2,6-dipyridyl)dihydropyridyl)benzene (**1**) and 5,5′-bis-(azanediyl)-oxalyl-diisophthalic acid (**2**). Single crystal X-ray diffraction analysis shows that **SOF-7** comprises **2** and 1,4-bis-(4-(3,5-dicyano-2,6-dipyridyl)pyridyl)benzene (**3**); the latter formed *in situ* from the oxidative dehydrogenation of **1**. **SOF-7** shows a three-dimensional four-fold interpenetrated structure with complementary O−H···N hydrogen bonds to form channels that are decorated with cyano and amide groups. **SOF-7** exhibits excellent thermal stability and solvent and moisture durability as well as permanent porosity. The activated desolvated material **SOF-7a** shows high CO_2 adsorption capacity and selectivity compared with other porous organic materials assembled solely through hydrogen bonding.

Porous framework materials, such as porous carbon,[1] zeolites,[2] metal−organic frameworks,[3] and porous organic frameworks,[4−7] have attracted intensive research interest due to their potential applications in molecular storage and separation. Porous organic framework materials have become competitive materials because of their low framework density resulting from the use of light elements (typically H, C, N, O, B) and their low toxicity as well as their controllable assembly through organic synthesis and crystal engineering.[4−7] For example, covalent organic frameworks (COFs)[6] or porous organic polymers (POPs) and polymers of intrinsic microporosity (PIMs) represent[7] a widely investigated family of porous organic materials that are typically prepared from organic coupling reactions of selected and/or designed precursors. However, the development of COFs/POPs/PIMs has been somewhat restricted by harsh reaction conditions, multistep syntheses, and the involvement of relatively expensive catalysts.

Supramolecular organic frameworks (SOFs) have recently been recognized as promising porous materials which are constructed from functional organic modules assembled via supramolecular interactions (e.g., hydrogen bonds, $\pi-\pi$ stacking, CH···π, and van der Waals interactions).[4,5] Special interest in SOF materials comes from the soft and flexible nature of their molecular interactions, the ease of manipulation of the modularity and functionality of the organic components, and the tunable guest selectivity achieved by decorating the pores with organic groups that can exploit specific interactions with different gas molecules. Moreover, SOF materials can be highly crystalline, which is an advantage not only for structural determination but also for investigation of structure−property relationships. However, upon guest removal many SOF materials undergo phase changes to give close-packed structures, lose porosity, and/or undergo structure collapse due to the relative weakness of the supramolecular interactions that underpin the framework structure.[8] We have targeted organic modules with favorable molecular configurations that promote the formation of spatial voids and permanent cavities, noting that cooperative functional groups play a key role in stabilizing molecular assemblies via both intramolecular and intermolecular interactions.[9]

SOF materials have been reported in which a single type of organic molecule crystallizes into a porous phase via supramolecular hydrogen-bonding interactions[5a−f] in which the resultant porous phase depends greatly on the solvents present. Specific intermolecular interactions such as hydrogen bonds

Scheme 1. Schematic View of the Organic Modules

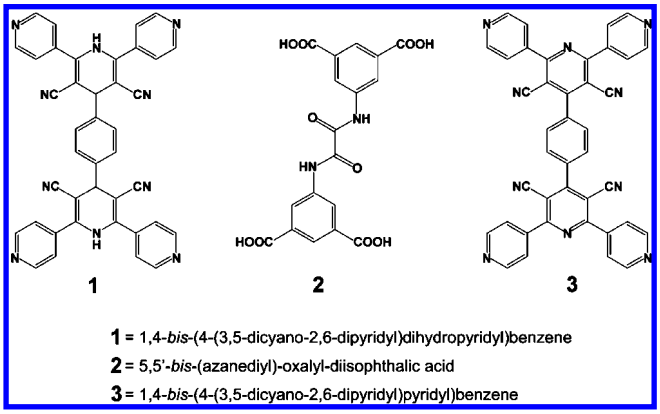

Received: June 30, 2014

   dx.doi.org/10.1021/ja506577g | J. Am. Chem. Soc. XXXX, XXX, XXX−XXX

can be optimized and balanced in two- and multicomponent materials via molecular recognition between functional organic modules.[10] In this context, we have adopted a binary design strategy in which two different hydrogen-bonding tectons assemble to form a stable porous network.

In this work, 1,4-bis-(4-(3,5-dicyano-2,6-dipyridyl)-dihydropyridyl)benzene (**1**) and 5,5′-bis-(azanediyl)-oxalyl-diisophthalic acid (**2**) (Scheme 1) have been chosen to build a binary SOF material for selective gas storage. Our approach is based upon the use of *exo*-pyridyl and carboxyl groups on two separate organic modules that give complementary directional hydrogen bonding and, at the same time, incorporate amide groups on **2** to give potential interactions with CO_2.[11]

Reaction of **1** and **2** in a 1:1 molar ratio in dimethylformamide (DMF) at 90 °C resulted in the formation of orange prismatic crystals of **SOF-7** after 72 h. This material is a solvated binary hydrogen-bonded cocrystal[9a,c,g,h] with overall formula $[(C_{18}H_{12}N_2O_{10})\cdot(C_{40}H_{20}N_{10})]\cdot 7DMF$ comprising a 1:1 combination of **2** and 1,4-bis-(4-(3,5-dicyano-2,6-dipyridyl)pyridyl)benzene (**3**), this latter species[9i] being formed *in situ* by oxidative dehydrogenation of **1**. A single crystal X-ray structure determination (Table S1) reveals that **SOF-7** crystallizes in the monoclinic space group *C*2/*c* and features a three-dimensional (3D), four-fold interpenetrating lattice containing channels decorated with cyano and amide groups (Figure 1a). The *exo*-carboxyl and pyridyl groups on **2** and **3**

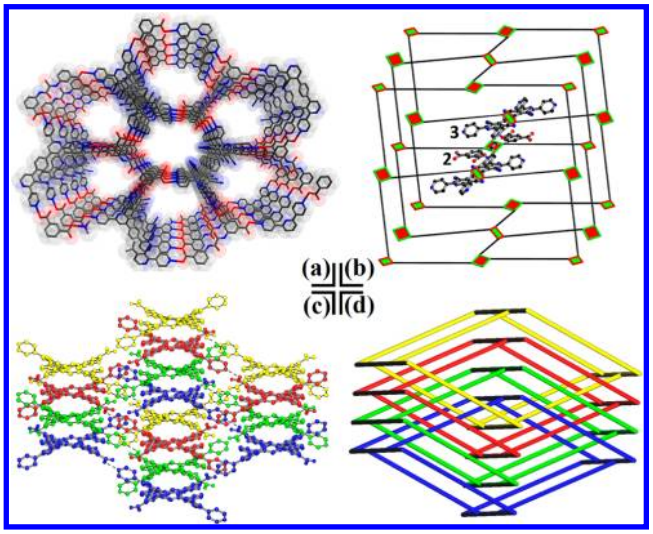

Figure 1. Views of **SOF-7** (a) the 3D structure along *a* axis; (b) the simplified **cds** net (red node, **2**; green node, **3**); (c) the four-fold interpenetrating framework; (d) a simplified schematic view of the four-fold interpenetrating **cds** nets.

contribute to the O−H···N hydrogen bonds which direct the self-assembly process. Moreover, the lateral amide in **2** and cyano group in **3** may offer potential binding sites for guest molecules to enhance gas uptake. The network can be regarded as a cocrystal rather than an organic salt since complete proton transfer between the carboxyl and pyridyl groups is not observed with two different C to O distances (C−OH = ∼1.31 Å; C═O = ∼1.21 Å) observed, consistent with protonation of the carboxyl group.[9g,h]

In **SOF-7**, each molecule of **2** interacts with four neighboring molecules of **3** through primary hydrogen bonds ($O_{carboxyl}$−H···$N_{pyridyl}$, 2.598(5), 2.599(4) Å) to form a 3D supramolecular organic network (Figure 1a). The guest DMF molecules reside within the channels of this material and interact with the internal amide groups in **2** via secondary hydrogen-bond interactions (N_{amide}−H···$O_{carbonyl}$, 2.890(5) Å). The network topology of **SOF-7** was analyzed using TOPOS[12] as a 6^5·8-**cds** ($CdSO_4$) net, reflecting a square topology (Figure 1b). This topology has been identified as one of the most frequently observed nets to show framework interpenetration.[13] This is also the case for **SOF-7** in which four identical **cds** nets interpenetrate to give an overall four-fold interpenetrating framework (Figure 1c,d). Π−π interactions are observed between two *exo*-pyridyl groups in **3** (∼3.077 Å) from adjacent single nets as well as between a central pyridyl moiety in **3** and a phenyl group in **2** (∼3.421 Å) from adjacent single nets. Despite this network interpenetration, the total solvent-accessible volume of **SOF-7** after removal of guest DMF molecules was estimated to be ∼48% as calculated using PLATON/VOID routine.[14] The thermal stability of the **SOF-7** framework was evaluated by thermogravimetric analysis (TGA), which showed a decomposition temperature of around 350 °C (Figure S1). The phase purity of the bulk sample of **SOF-7** was confirmed by powder X-ray diffraction (PXRD, Figure S2). The DMF molecules within the pores of **SOF-7** were exchanged with acetone, and the acetone-exchanged sample degassed under dynamic vacuum at 100 °C for 24 h to afford the activated, desolvated sample **SOF-7a**. **SOF-7a** retains its structural integrity and crystallinity upon solvent exchange as well as upon removal of guest molecules, as confirmed by PXRD patterns (Figure S2), which revealed a highly robust framework. Moreover, the desolvated sample **SOF-7a** exhibited excellent structural durability toward both common organic solvents and water (Figure S3).

The permanent porosity of **SOF-7a** was confirmed by gas adsorption studies. The results clearly show that **SOF-7a** exhibits selective adsorption for CO_2 over N_2, H_2 and CH_4 (Figures 2a,b, and S4). The N_2 adsorption isotherm of **SOF-7a**

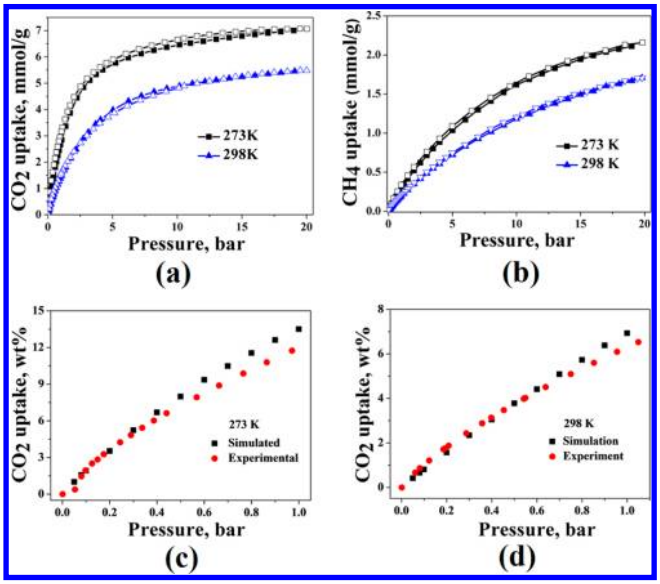

Figure 2. CO_2 isotherms for **SOF-7a** at 273 K (black) and 298 K (blue) in the pressure range 0−20 bar (a); CH_4 isotherms for **SOF-7a** at 273 K (black) and 298 K (blue) in the pressure range 0−20 bar (b); experimental (red) and simulated (black) CO_2 isotherms up to 1 bar at 273 K (c); experimental (red) and simulated (black) CO_2 isotherms up to 1 bar at 298 K (d).

dx.doi.org/10.1021/ja506577g | J. Am. Chem. Soc. XXXX, XXX, XXX−XXX

at 77 K displays restricted adsorption behavior (Figure S4), with the Brunauer–Emmett–Teller (BET) surface area of **SOF-7a** calculated from N_2 adsorption isotherm at 77 K being much lower than expected (21.03 $m^2 \cdot g^{-1}$). However, the CO_2 isotherm recorded at 273 K reveals a reversible type-I adsorption behavior and gives an expected BET surface area based upon the crystal structure of 900.0 $m^2 \cdot g^{-1}$ (Figure S5). Furthermore, the pore volume estimated from the N_2 adsorption isotherm (0.097 $cm^3 \cdot g^{-1}$) is significantly lower than the value estimated from the CO_2 adsorption isotherm (0.233 $cm^3 \cdot g^{-1}$) using non-local density functional theory modeling. Interactions between N_2 and the channel windows of **SOF-7a** at 77 K could hinder the diffusion of N_2 into the material; restricted N_2 uptake but higher type-I CO_2 uptake has been observed previously in materials with pore sizes larger than the kinetic diameter of N_2.[5b,15] Thus, in this case, the BET surface area and the pore size distribution for **SOF-7a** calculated from the CO_2 adsorption isotherm were 900.0 $m^2 \cdot g^{-1}$ and 13.6 Å (Figure S6), respectively, in good accordance with the channel window of ~13.5 × 14 Å calculated from the single crystal X-ray data.

SOF-7a was tested for CO_2 adsorption at different temperatures. **SOF-7a** shows reversible CO_2 adsorption with CO_2 capacities of 12.54 wt % (2.85 $mmol \cdot g^{-1}$) and 6.53 wt % (1.49 $mmol \cdot g^{-1}$) at 273 and 293 K at 1 bar, respectively (Figure 2a). High-pressure (20 bar) CO_2 adsorption of **SOF-7a** gives the total amount of 31.09 wt % (7.07 $mmol \cdot g^{-1}$) and 24.12 wt % (5.48 $mmol \cdot g^{-1}$) at 273 and 293 K (Figure 2a), respectively. The CO_2 adsorption capacity of **SOF-7a** at 273 K and 1 bar is comparable to some of the best performing single component SOF materials;[4a−c,5b−d] for example, triptycene-tris-(benzimidazolone) absorbs 15.9 wt % CO_2 at 273 K and 1 bar[5d] (Table S2). The heat of adsorption for CO_2 (Q_{st}) was calculated via the Clausius–Clapeyron equation using CO_2 isotherms at 273 and 298 K (Figure S7) and was found to be 21.6 $kJ \cdot mol^{-1}$ at zero loading, which is slightly lower than previously reported single component SOF materials.[4a−c,5b−d]

Uptake of methane by **SOF-7a** was tested at different pressures (up to 20 bar) and temperatures (273 and 298 K) (Table S3), the isotherms showing reversible CH_4 uptake of 0.47 wt % (0.29 $mmol \cdot g^{-1}$) and 0.35 wt % (0.22 $mmol \cdot g^{-1}$) at 1 bar, and 3.38 wt % (2.11 $mmol \cdot g^{-1}$) and 2.74 wt % (1.71 $mmol \cdot g^{-1}$) at 20 bar (Figure 2b). The CH_4 uptake of **SOF-7a** at 16 bar and 298 K (1.54 $mmol \cdot g^{-1}$) is comparable to that of **SOF-1a** (1.43 $cm^3 \cdot g^{-1}$). Strikingly, however, **SOF-7a** adsorbs ~70% more of CO_2 than **SOF-1a** at 16 bar and 298 K (5.30 vs 3.08 $mmol \cdot g^{-1}$). In comparison with the selectivity of CO_2 over CH_4 calculated for **SOF-1a** from Henry's Law constant, **SOF-7a** shows significantly higher CO_2/CH_4 selectivity of 9.13 at 298 K and 1 bar, compared with 4.24 (at 298 K and 1 bar) for **SOF-1a** and 14.2 for **SOF-7a** and 5.60 for **SOF-1a** (at 273 K and 1 bar).

In order to analyze further the gas adsorption properties of **SOF-7a**, grand canonical Monte Carlo (GCMC) simulations of CO_2 adsorption were performed (see ESI). The results of GCMC simulations of CO_2 adsorption in **SOF-7a** are in good agreement with the experimental data at 273 and 298 K at up to 1 bar (Figure 2c,d). Moreover, *in situ* PXRD patterns of CO_2-loaded **SOF-7a** were studied in order to monitor the possible dynamic structural changes related to CO_2 adsorption. The *in situ* PXRD patterns remain essentially the same at 273 and 298 K up to 1 bar (Figure S8), suggesting that there are no significant structural changes or deterioration; this is consistent with the excellent match between simulated and experimental CO_2 isotherms for **SOF-7a** at pressures of up to 1 bar.

GCMC simulations for CO_2 adsorption at different pressures have also been conducted to analyze potential CO_2 binding sites on the framework material of **SOF-7a**. Density functional calculations (DFT) have yielded binding energies (BE) and reveal the configurations corresponding to the strongest binding of CO_2 in **SOF-7a** (Table S4). The three most preferred binding sites for CO_2 in **SOF-7a** have been identified (Figure 3): the most stable configuration (BE = −35.19 $kJ \cdot mol^{-1}$) is characterized by strong N–H···O@CO_2 hydrogen-bond interaction; the second most stable configuration (BE = −31.53 $kJ \cdot mol^{-1}$) is characterized by one N–H···O@CO_2 hydrogen bond and two electrostatic attractions between the carbon of CO_2 (q = 0.40 |e|) and the electronegative nitrogen atoms of the linker (q = −0.20 |e|); the third most stable configuration (BE = −29.75 $kJ \cdot mol^{-1}$) corresponds to a CO_2 location near the amide group of the linker, stabilized by N–H···O@CO_2 and C–H···O@CO_2 hydrogen-bonding interactions and electrostatic interaction between C@CO_2 and oxygen atoms in the linker. The calculation thus confirms that the amide and cyano groups in **2** and **3** contribute significantly to the highly selective binding of CO_2 in **SOF-7a**.

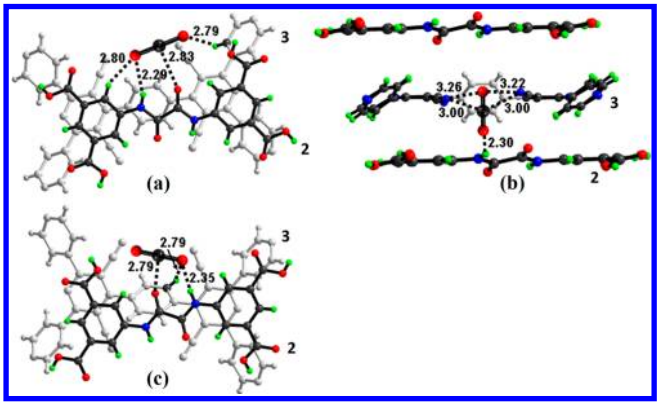

Figure 3. Binding of CO_2 molecules to **SOF-7a** as determined by GCMC simulations and DFT calculations (labeled distances are in Å): (a) CO_2 interacting with the amide group in **2** in a parallel position to also form N–H···O hydrogen bonds to **3**; (b) CO_2 interacting with the amide group in **2** in a perpendicular position to also form N–H···O hydrogen bonds to **3**; (c) CO_2 interacting with the cyano groups in **3** in a parallel position to also form N–H···O hydrogen bonds to **2**.

In summary, we have demonstrated a new strategy using two different organic building blocks incorporating complementary hydrogen bonding donor–acceptor motifs to form new SOF materials via the formation of cocrystals. **SOF-7** features a 3D four-fold interpenetrating structure incorporating channels decorated with cyano and amide groups. **SOF-7** is crystalline, highly robust, and shows permanent porosity. Appropriate functionalization of the organic building blocks favors not only the successful isolation of **SOF-7** but also excellent CO_2 adsorption capacity and selectivity. GCMC simulation confirms the role of these functional groups as favorable binding sites for CO_2 molecules, thereby enhancing CO_2/CH_4 selectivity. To our knowledge, **SOF-7a** represents the first binary hydrogen-bonded supramolecular organic framework material to exhibit gas adsorption. The design strategy described herein opens up new possibilities for the flexible synthesis of not only new modified and extended binary systems but may also be

dx.doi.org/10.1021/ja506577g | J. Am. Chem. Soc. XXXX, XXX, XXX–XXX

programmed and extended toward tertiary and higher component porous assemblies.

■ ASSOCIATED CONTENT

Supporting Information

Experimental details and supporting cif files, figures, graphs, and tables. This material is available free of charge via the Internet at http://pubs.acs.org.

■ AUTHOR INFORMATION

Corresponding Author

M.Schroder@nottingham.ac.uk

Notes

The authors declare no competing financial interest.

■ ACKNOWLEDGMENTS

We thank the EPSRC and the University of Nottingham for funding, and the EPSRC National Crystallography Service and Diamond Light Source (Beamline I11) for data collection. We acknowledge the Royal Society and Sino-British Fellowship Trust for an Incoming Fellowship (to J.L.), the Royal Commission for Jubail and Yanbu, Jubail University College, Kingdom of Saudi Arabia, for a Ph.D. Fellowship (to N.H.A.), and Conacyt, Mexico (to C.P.K.) for funding. M.S. gratefully acknowledges receipt of an ERC Advanced Grant and J.L. and M.S. thank the NSFC-RS International Exchanges Scheme (2011 China Costshare project based on NSFC-21001105) for financial support.

■ REFERENCES

(1) (a) Raymundo-Piñero, E.; Cazorla-Amorós, D.; Salinas-Martinez de Lecea, C.; Linares-Solano, A. *Carbon* **2000**, *38*, 335. (b) Zhao, X.; Villar-Rodil, S.; Fletcher, A. J.; Thomas, K. M. *J. Phys. Chem. B* **2006**, *110*, 9947. (c) Yang, Z.; Xia, Y.; Mokaya, R. *J. Am. Chem. Soc.* **2007**, *129*, 1673. (d) Hao, G.-P.; Li, W.-C.; Qian, D.; Wang, G.-H.; Zhang, W.-P.; Zhang, T.; Wang, A.-Q.; Schüth, F.; Bongard, H.-J.; Lu, A.-H. *J. Am. Chem. Soc.* **2011**, *133*, 11378. (e) Hao, G.-P.; Li, W.-C.; Qian, D.; Lu, A.-H. *Adv. Mater.* **2010**, *22*, 853. (f) Sevilla, M.; Valle-Vigón, P.; Fuertes, A. B. *Adv. Funct. Mater.* **2011**, *21*, 2781. (g) Sevilla, M.; Fuertes, A. B. *Energy Environ. Sci.* **2011**, *4*, 1765.

(2) (a) Brändle, M.; Sauer, J. *J. Am. Chem. Soc.* **1998**, *120*, 1556. (b) Hudson, M. R.; Queen, W. L.; Mason, J. A.; Fickel, D. W.; Lobo, R. F.; Brown, C. M. *J. Am. Chem. Soc.* **2012**, *134*, 1970. (c) Shang, J.; Li, G.; Singh, R.; Gu, Q.; Nairn, K. M.; Bastow, T. J.; Medhekar, N.; Doherty, C. M.; Hill, A. J.; Liu, J. Z.; Webley, P. A. *J. Am. Chem. Soc.* **2012**, *134*, 19246.

(3) (a) Zhang, J. P.; Chen, X. M. *J. Am. Chem. Soc.* **2009**, *131*, 5516. (b) Sumida, K.; Rogow, D. L.; Mason, J. A.; McDonald, T. M.; Bloch, E. D.; Herm, Z. R.; Bae, T.-H.; Long, J. R. *Chem. Rev.* **2012**, *112*, 724. (c) Millward, A. R.; Yaghi, O. M. *J. Am. Chem. Soc.* **2005**, *127*, 17998. (d) Yang, S.; Lin, X.; Lewis, W.; Suyetin, M.; Bichoutskaia, E.; Parker, J.; Tang, C. C.; Allan, D. R.; Rizkallah, P. J.; Hubberstey, P.; Champness, N. R.; Thomas, K. M.; Blake, A. J.; Schröder, M. *Nat. Mater.* **2012**, *11*, 710. (e) Yang, S.; Sun, J.; Ramirez-Cuesta, A. J.; Callear, S. K.; David, W. I. F.; Anderson, D.; Newby, R.; Blake, A. J.; Parker, J. E.; Tang, C. C.; Schröder, M. *Nat. Chem.* **2012**, *4*, 887.

(4) (a) Lim, S.; Kim, H.; Selvapalam, N.; Kim, K.-J.; Cho, S. J.; Seo, G.; Kim, K. *Angew. Chem., Int. Ed.* **2008**, *47*, 3352. (b) Kim, H.; Kim, Y.; Yoon, M.; Lim, S.; Park, S. M.; Seo, G.; Kim, K. *J. Am. Chem. Soc.* **2010**, *132*, 12200. (c) Tian, J.; Ma, S.; Thallapally, P. K.; Fowler, D.; McGrail, B. P.; Atwood, J. L. *Chem. Commun.* **2011**, *47*, 7626. (d) Hasell, T.; Schmidtmann, M.; Cooper, A. I. *J. Am. Chem. Soc.* **2011**, *133*, 14920. (e) Bojdys, M. J.; Briggs, M. E.; Jones, J. T. A.; Adams, D. J.; Chong, S. Y.; Schmidtmann, M.; Cooper, A. I. *J. Am. Chem. Soc.* **2011**, *133*, 16566. (f) Hasell, T.; Chong, S. Y.; Jelfs, K. E.; Adams, D. J.; Cooper, A. I. *J. Am. Chem. Soc.* **2012**, *134*, 588.

(5) (a) Sozzani, P.; Bracco, S.; Comotti, A.; Ferretti, L.; Simonutti, R. *Angew. Chem., Int. Ed.* **2005**, *44*, 1816. (b) Yang, W.; Greenaway, A.; Lin, X.; Matsuda, R.; Blake, A. J.; Wilson, C.; Lewis, W.; Hubberstey, P.; Kitagawa, S.; Champness, N. R.; Schröder, M. *J. Am. Chem. Soc.* **2010**, *132*, 14457. (c) He, Y.; Xiang, S.; Chen, B. *J. Am. Chem. Soc.* **2011**, *133*, 14570. (d) Mastalerz, M.; Oppel, I. M. *Angew. Chem., Int. Ed.* **2012**, *51*, 5252. (e) Luo, X.-Z.; Jia, X.-J.; Deng, J.-H.; Zhong, D.-C. *J. Am. Chem. Soc.* **2013**, *135*, 11684. (f) Li, P.; He, Y.; Guang, J.; Weng, L.; Zhao, J. C.-G.; Xiang, S.; Chen, B. *J. Am. Chem. Soc.* **2014**, *136*, 547. (g) Yamamoto, A.; Hamada, T.; Hisaki, I.; Miyata, M.; Tohnai, N. *Angew. Chem., Int. Ed.* **2013**, *52*, 1709.

(6) (a) Côté, A. P.; Benin, A. I.; Ockwig, N. W.; O'Keeffe, M.; Matzger, A. J.; Yaghi, O. M. *Science* **2005**, *310*, 1166. (b) El-Kaderi, H. M.; Hunt, J. R.; Mendoza-Cortés, J. L.; Côté, A. P.; Taylor, R. E.; O'Keeffe, M.; Yaghi, O. M. *Science* **2007**, *316*, 268. (c) Ding, X.; Chen, L.; Honsho, Y.; Feng, X.; Saengsawang, O.; Guo, J.; Saeki, A.; Seki, S.; Irle, S.; Nagase, S.; Parasuk, V.; Jiang, D. *J. Am. Chem. Soc.* **2011**, *133*, 14510. (d) Ding, S.-Y.; Wang, W. *Chem. Soc. Rev.* **2013**, *42*, 548.

(7) For example see: (a) Ben, T.; Ren, H.; Ma, S.; Cao, D.; Lan, J.; Jing, X.; Wang, W.; Xu, J.; Deng, F.; Simmons, J. M.; Qiu, S.; Zhu, G. *Angew. Chem., Int. Ed.* **2009**, *48*, 9457. (b) Trewin, A.; Cooper, A. I. *Angew. Chem., Int. Ed.* **2010**, *49*, 1533. (c) Ben, T.; Pei, C.; Zhang, D.; Xu, J.; Deng, F.; Jing, X.; Qiu, S. *Energy Environ. Sci.* **2011**, *4*, 3991. (d) Dawson, R.; Stöckel, E.; Holst, J. R.; Adams, D. J.; Cooper, A. I. *Energy Environ. Sci.* **2011**, *4*, 4239. (e) Dawson, R.; Cooper, A. I.; Adams, D. *J. Prog. Polym. Sci.* **2012**, *37*, 530. (f) Msayib, K. J.; Book, D.; Budd, P. M.; Harris, K. D. M.; Helliwell, M.; Tedds, S.; Warren, J. E.; Xu, M. C.; McKeown, N. B. *Angew. Chem., Int. Ed.* **2009**, *48*, 3273. (g) Bezzu, C. G.; Carta, M.; Tonkins, A.; Jansen, J. C.; Bernardo, P.; Bazzarelli, F.; McKeown, N. B. *Adv. Mater.* **2012**, *24*, 5930.

(8) (a) Dalgarno, S. J.; Thallapally, P. K.; Barbour, L. J.; Atwood, J. L. *Chem. Soc. Rev.* **2007**, *36*, 236. (b) Maspoch, D.; Ruiz-Molina, D.; Veciana, J. *Chem. Soc. Rev.* **2007**, *36*, 770.

(9) (a) Kuduva, S. S.; Craig, D. C.; Nangia, A.; Desiraju, G. R. *J. Am. Chem. Soc.* **1999**, *121*, 1936. (b) Vishweshwar, P.; McMahon, J. A.; Peterson, M. L.; Hickey, M. B.; Shattock, T. R.; Zaworotko, M. J. *Chem. Commun.* **2005**, *41*, 4601. (c) Braga, D.; Grepioni, F. *Chem. Commun.* **2005**, *41*, 3635. (d) Gilli, P.; Pretto, L.; Bertolasi, V.; Gilli, T. *Acc. Chem. Res.* **2009**, *42*, 33. (e) Khan, M.; Enkelmann, V.; Brunklaus, G. *J. Am. Chem. Soc.* **2010**, *132*, 5254. (f) Berná, J.; Alajarín, M.; Orenes, R.-A. *J. Am. Chem. Soc.* **2010**, *132*, 10741. (g) Cheney, M. L.; Weyna, D. R.; Shan, N.; Hanna, M.; Wojtas, L.; Zawarotko, M. J. *Cryst. Growth Des.* **2010**, *10*, 4401. (h) Schultheiss, N.; Lorimer, K.; Wolfe, S.; Desper, J. *CrystEngComm* **2010**, *12*, 742. (i) Ghozlan, S. A. S.; Hassanien, A. Z. A. *Tetrahedron* **2002**, *58*, 9423.

(10) (a) Aakeröy, C. B.; Beatty, A. M.; Helfrich, B. A. *Angew. Chem., Int. Ed.* **2001**, *40*, 3240. (b) Bhogala, B. R.; Basavoju, S.; Nangia, A. *Cryst. Growth Des.* **2005**, *5*, 1683. (c) Martí-Rujas, J.; Colombo, L.; Lü, J.; Dey, A.; Terraneo, G.; Metrangolo, P.; Pilati, T.; Resnati, G. *Chem. Commun.* **2012**, *48*, 8207.

(11) (a) Dincă, M.; Long, J. R. *Angew. Chem., Int. Ed.* **2008**, *47*, 6766. (b) Dietzel, P. D. C.; Besikiotis, V.; Blom, R. *J. Mater. Chem.* **2009**, *19*, 7362. (c) Zheng, B.; Bai, J.; Duan, J.; Wojtas, L.; Zaworotko, M. J. *J. Am. Chem. Soc.* **2011**, *133*, 748. (d) Duan, J.; Yang, Z.; Bai, J.; Zheng, B.; Li, Y.; Li, S. *Chem. Commun.* **2012**, *48*, 3058.

(12) Blatov, V. A. *IUCr Computing Commission Newsletter*; International Union of Crystallography: Chester, England, 2006; Vol. 7, p 4; see also http://www.topos.ssu.samara.ru

(13) Alexandrov, E. V.; Blatov, V. A.; Kochetkov, A. V.; Proserpio, D. M. *CrystEngComm* **2011**, *13*, 3947.

(14) Spek, A. L. PLATON, *Acta Crystallogr., Sect. D: Biol. Crystallogr.* **2009**, *65*, 148.

(15) (a) Maji, T. K.; Matsuda, R.; Kitagawa, S. *Nat. Mater.* **2007**, *6*, 142. (b) Ok, K. M.; Sung, J.; Hu, G.; Jacobs, R. M. J.; O'Hare, D. *J. Am. Chem. Soc.* **2008**, *130*, 3762.

Electronic Supporting Information

A Robust Binary Supramolecular Organic Framework (SOF) with High CO_2 Adsorption and Selectivity

Jian Lü,[a,b] Cristina Perez-Krap,[a] Mikhail Suyetin,[a] Nada Al Smail,[a] Yong Yan,[a] Sihai Yang,[a] William Lewis,[a] Elena Bichoutskaia,[a] Chiu C. Tang,[c] Alexander J. Blake,[a] Rong Cao[b] and Martin Schröder*[a]

[a]*School of Chemistry, University of Nottingham, University Park, Nottingham NG7 2RD, UK. Fax: +44 115 951 3563; E-mail: M.Schroder@nottingham.ac.uk*

[b]*State Key Laboratory of Structural Chemistry, Fujian Institute of Research on the Structure of Matter, Chinese Academy of Sciences, Fujian, Fuzhou 350002, P. R. China*

c Diamond Light Source, Harwell Science and Innovation Campus, Didcot, OX11 0DE, UK.

**Corresponding author.*

Chemicals and General methods

Commercially available reagents and organic solvents were used as received without further purification. Elemental analyses (C, H, and N) were performed on a CE-440 elemental analyzer. Infrared (IR) spectra were recorded with a PerkinElmer Spectrum One with KBr pellets in the range 400–4000 cm^{-1}, or on a Nicolet iS5 FT-IR spectrophotometer in the range of 550-4000 cm^{-1} using the attenuated total reflectance (ATR) mode. ^1H NMR spectra were recorded on a Bruker DPX-400 spectrometer. Thermal gravimetric analyses (TGA) were performed under a flow of nitrogen (20 $mL \cdot min^{-1}$) with a heating rate of 10 °C·min^{-1} using a TA SDT-600 thermogravimetric analyzer. X-ray powder diffraction (PXRD) measurements were carried out at room temperature on a PANalytical X'Pert PRO diffractometer using Cu-Kα radiation (λ = 1.5418 Å) at 40 kV, 40 mA, at a scan speed of 0.02°/s and a step size of 0.005° in 2θ. N_2, H_2, CO_2 and CH_4 isotherms were recorded using an *IGA* gravimetric adsorption apparatus (Hiden) at the University of Nottingham in a clean ultra-high vacuum system with a diaphragm and turbo pumping system. Before measurement, about 60 mg solvent-exchanged sample was loaded into the sample basket within the adsorption instrument and then degassed under dynamic vacuum at 100 °C for 24 hours to obtain the fully desolvated sample.

Experimental

Synthesis of 3-Amino-3-(4-pyridinyl)-propionitrile[S1]: 4-Cyanopyridine (104 mg, 1.0 mmol), in MeCN (82 mg, 2.0 mmol), and potassium *tert*-butoxide (336 mg, 3.0 mmol) were added to toluene (40 mL) and the reaction mixture stirred at ambient temperature for 48 h. Saturated $NaHCO_3$ solution (200 mL) was used to quench the reaction, and the resultant solid crude product of 3-amino-3-(4-pyridinyl)-propionitrile was collected by filtrations and washed three times with NaCl solution and dried in air. Yield: 76%. ^1H NMR (DMSO-d^6): 8.63 (d, J = 6.3 Hz, 2H, *2*,*6*-Pyridyl-H); 7.57 (d, J = 6.0 Hz, 2H, *3*,*5*-Pyridyl-H); 7.01 (s, 2H, NH), 4.4 (s, 1H, =C-H) ppm. HRMS (EI-): *m*/*z* 439.0403 $[M+H]^+$. IR (KBr, υ_{max}, cm^{-1}): 2801 (w), 2759 (w), 2256 (m), 2194 (s), 1942 (m), 1670 (s), 1593 (s),

1530 (s), 1502 (s), 1425 (s), 1335 (m), 1271 (m), 1222 (m), 1146 (m), 1069 (m), 992 (s), 874 (m), 839 (s), 670 (s), 650 (s), 609 (s), 573 (s). Elemental analysis for $C_8H_7N_3$ (found/calcd): C, 66.15/66.19; H, 4.83/4.86; N, 28.94/28.95.

Synthesis of 1,4-*bis*-(4-(3,5-dicyano-2,6-dipyridyl)dihydropyridyl)benzene[S1a] **(1)**: 3-Amino-3-(4-pyridinyl)-propionitrile (580 mg, 4.0 mmol) and 1,3-benzenedialdehyde (134 mg, 1.0 mmol) were added to acetic acid (10 mL) under N_2 and the reaction mixture refluxed at 120 ºC for 48 h. The light yellow precipitate of **1** was collected by filtration and washed with hot acetic acid, EtOH, and distilled water and dried in air. Yield: 61% ^{1}H NMR (DMSO-d^6): 10.4 (s, 2H, dihydropyridyl-NH), 8.7 (d, J = 4.7 Hz, 8H, Py-H), 7.7 (d, J = 4.7 Hz, 8H, Py-H); 7.65 (s, 4H, Ar-H), 4.9 (s, 2H, dihydropyridyl-CH) ppm. HRMS (EI-): m/z 643.21 $[M+H]^+$. IR (KBr, υ_{max}, cm^{-1}): 2205 (s), 1756 (w), 1718 (m), 1645 (m), 1599 (s), 1550 (m), 1516 (s), 1417 (m), 1345 (m), 1295 (s), 1273 (m), 1246 (w), 1215 (m), 1189 (w), 1155 (w) 1071 (w), 999 (w), 831 (m), 801 (w), 744 (w), 694 (w), 668 (w), 653 (w), 591 (m), 521 (w). Elemental analysis for $C_{40}H_{24}N_{10}$ (found/calcd): C, 74.80/74.52; H, 3.96/3.75; N, 21.22/21.73.

This reaction is very similar to that previously reported for the synthesis of **3**.[S1b] We were however unable to prepare signifucant amounts of **3** directly by this published route, and in our hands the synthesis of **1** was more reliable and generated the desired products.

Synthesis of 5,5'-*Bis*-(azanediyl)-oxalyl-diisophthalic acid[S2] **(2)**: A solution of 5-aminoisophthalic acid (6.53g, 34.2mmol) in anhydrous THF (50 mL) was cooled at 0 °C. A solution of oxalyl chloride (1.0 mL, 11.4 mmol) in anhydrous THF (100mL) was added dropwise to the above solution over 1 h, during which a precipitate formed almost immediately. Triethylamine (1.0 mL, 7.2 mmol) was slowly added after 1 h and the mixture was stirred overnight at room temperature. 2M HCl (200 mL) was then added and the white precipitate of **2** was filtered and washed with water, and recrystallized

from MeOH. The product was further washed with MeOH and diethyl ether and dried under vacuum to afford a white powder. Yield: 58%. ^{1}H NMR (DMSO-d^6): 13.08 (s, 4H, COOH); 11.26 (s, 2H, NH); 8.72 (d, J = 1.2 Hz, 4H, Ar-H); 8.26 (t, J = 1.2 Hz, 2H, Ar-H). ATR FT-IR (υ_{max}, cm^{-1}): 2158 (w), 1974 (w), 1716(s), 1681(s), 1653(s), 1558 (m), 1540 (s), 1456 (m), 1387 (s), 1301(m), 1275 (s), 1185 (w), 952 (m), 841(m), 758 (s), 728 (s), 670 (m). HRMS (EI-): m/z 439.0403 [M+Na]$^+$, 434.0838 [M+H_4N]$^+$, 415.0401 [M-H]$^-$. Elemental analysis for $C_{18}H_{12}N_2O_{10}$ (found/calcd): C, 51.93/51.47; H, 2.90/3.05; N, 6.73/6.56.

Synthesis of [($C_{18}H_{12}N_2O_{10}$)·($C_{40}H_{20}N_{10}$)]·7DMF (SOF-7): 1,4-*Bis*-(4-(3,5-dicyano-2,6-dipyridyl)dihydropyridyl)benzene (**1**) (33 mg, 0.05 mmol) and 5,5'-*bis*-(azanediyl)-oxalyl-diisophthalic acid (**2**) (21 mg, 0.05 mmol) were added to DMF (3mL). The reaction mixture was transferred into a 15 mL pressure tube and heated in oil bath at 90 °C and autogenous pressure for 3 days. Orange crystals were collected by filtration and washed with cold DMF to give pure phase of **SOF-7**. Yields: *ca*. 58%. IR (KBr, υ_{max}, cm^{-1}): 2459 (w), 2359 (w), 2231 (w) 1712 (s), 1662 (s), 1598 (m), 1558 (w), 1530 (m), 1392 (m), 1251 (s), 1101(m), 1060 (m), 1051 (m), 841(m), 800 (w), 764 (m), 686 (w), 659 (w), 609 (w), 572 (w), 499 (w). Elemental analysis for $C_{79}H_{81}N_{19}O_{17}$ (**SOF-7**, found/calcd): C, 60.49/61.31; H, 5.20/4.48; N, 16.97/16.61; for $C_{58}H_{32}N_{12}O_{10}$ (**SOF-7a**, found/calcd): C, 65.86/63.97; H, 3.05/3.18; N, 15.89/15.63.

Sample activation: As-prepared **SOF-7** was exchanged with acetone, and degassed under dynamic vacuum at 100 °C for 24 hours to afford the activated desolvated sample **SOF-7a**. **SOF-7a** retains its crystallinity and framework integrity as confirmed by PXRD (Figure S2). Moreover, the desolvated sample **SOF-7a** exhibits excellent durability towards both common organic solvents and water, even in boiling water (Figure S3). Recovery of **SOF-7a** sample as a crystalline material after gas adsorption experiments was realized by soaking the material in acetone or ethanol followed by the above activation (Figure S3).

Crystallography

Single crystal X-ray data was collected on Agilent GV1000 X-ray diffractometer at the University of Nottingham. Details of the data collection are included in the CIF. The structure was solved by direct methods and developed by difference Fourier techniques, both using the SHELXL software package.[S3] The hydrogen atoms of the ligands were placed geometrically and refined using a riding model. The unit cell volume includes a large region of disordered solvent which could not be modeled as discrete atomic sites. We therefore employed PLATON/SQUEEZE[S4] to calculate the contribution of the solvent region to the diffraction and thereby produced a set of solvent-free diffraction intensities.

Heats of Adsorption

The heats of adsorption (Q_{st}) were calculated using the Clausius Clapeyron equation (**1**) for CO_2 for isotherms at 273K and 293K and were solved by a virial-type equation (**2**).

$$\frac{d\ln(p)}{d(1/T)} = -\frac{\Delta H}{R} \qquad (\mathbf{1})$$

Where p is pressure, T is the temperature, R is the real gas constant;

$$\ln(n/p) = A_0 + A_1 n + A_2 n^2 + ... \qquad (\mathbf{2})$$

Where p is the pressure, n is the amount adsorbed, A_i is *Virial* coefficients, and i represents the number of coefficients required to adequately describe the isotherms with low uptakes.

Tóth method (Table S4)

The non-linear equation (**3**) was used

$$n = n_{sat}\left(b^{1/t}/1 + b^{t}\right)^{1/t} \qquad (\mathbf{3})$$

where n is the uptake in mmol·g^{-1}, n_{sat} is the saturation uptake mmol·g^{-1}, t and b are parameters which are specific for adsorbate-adsorbant pairs. The value of parameter t is usually less than unity

and is said to characterize the system heterogeneity. The Henry's law constant K_H, quantifies the extent of the adsorption of a given adsorbate by a solid. For the Tóth isotherm, the Henry's law constant is defined by the following equation (**4**):

$$K_H \lim_{p \to 0} \left(\frac{dn}{dp}\right) = b^{1/t} n_{sat} \qquad (4)$$

Dubinin Asthakov Method

In order to determine the pore size distribution, the CO_2 adsorption isotherm at 273K was fitted using the *Dubinin Asthakov* (D.A) model (Eq. **5**).

$$n_{ad} = n_p \exp\left(-\frac{RT}{E_0} \ln\left[\frac{P_0}{P}\right]\right)^n \qquad (5)$$

where n_{ad} is the experimental adsorption, n_p is the microporous limit capacity and E_0 is the adsorption characteristic energy based on pore filling mechanism. Equation fits calculated data to experimental isotherm by varying two parameters, E_0 and n. E_0 is average adsorption energy that is directly related to average pore diameter, and n is an exponent that controls the width of the resulting pore size distribution.

	E_0	n	Surface Area	Pore Volume
SOF-7a	8.84 kJ·mol^{-1}	2.7	913 m^2·g^{-1}	0.32 cm^3·g^{-1}

Grand Canonical Monte Carlo (GCMC) simulations

Grand Canonical Monte Carlo (GCMC) simulations were performed to analyse the adsorption of CO_2 in **SOF-7a**. The simulation parameters for CO_2 were taken from the TraPPE force field.[S5] The CO_2 molecule was assumed to have the C−O bond length of 1.16 Å, and three charged Lennard-Jones interaction sites with the following parameters: σ_O = 3.05 Å, ε_O/k_B = 79 K for oxygen atom, and σ_C = 2.80 Å and ε_C/k_B = 27 K for carbon atom. A point charge of +0.7was placed at the centre of mass of carbon atom and a point charge of −0.35 was placed at oxygen atom. Atomic parameters for the framework structure were described by the OPLS-AA force

field[S6] and for oxygen atoms present in **SOF-7a**, the modelling atomic parameters were taken from and adjusted for a correct description of the interaction between guest CO_2 molecules and the host SOF.[S7] The supercell used to represent **SOF-7a** in simulations contained 5 (5x1x1) unit cells, and periodic boundary conditions were applied to the supercell. The fugacity was calculated from the Peng-Robinson equation of state,[S8] and the Lennard-Jones (LJ) potential used to describe the Van der Waals interactions with a cut-off distance of 12.8 Å. The partial charges on atoms of the **SOF-7a** were computed using the CHELPG approach and the B3LYP/6-31G* level of density functional theory (DFT), as implemented in Q-Chem quantum chemistry package.[S9] The GCMC simulations were performed with *MUSIC* simulation suite[S10] and included $2 \cdot 10^7$ step equilibration period followed by $2 \cdot 10^7$ step production run.

Binding energy calculations

Density functional calculations (DFT), as implemented in the Q-Chem quantum chemistry package, was employed to analyze in detail the strength of the preferred adsorption sites in **SOF-7a**, calculate the binding energies (BE) between CO_2 molecule and the framework, and reveal and describe configurations corresponding to the strongest binding. The calculations were performed in two-stages: the geometry optimization was carried out at the B3LYP/6-31G** level of theory with dispersion correction taken into account,[S11] and the binding energies were subsequently calculated at the higher B3LYP/6-311++G** level with dispersion correction as follows:

$$\mathbf{BE = E(complex) - E(linker) - E_{opt}(CO_2)}$$

The BE was corrected for basis set superposition error (BSSE). Several energy minimum configurations revealed strong binding, and their properties are summarized in the Table S4.

Table S1 Crystallographic data for **SOF-7**

Compounds	**SOF-7**
Chemical formula	$C_{79}H_{81}N_{19}O_{17}$
Formula mass	1568.62
Crystal system	Monoclinic
Space group	*C*2/*c*
a/Å	7.65676(19)
b/Å	30.1426(8)
c/Å	34.5158(8)
α/°	90.00
β/°	93.900(2)
γ/°	90.00
Cell volume/Å^3	7947.6(3)
Z	4
Reflections collected	46769
Independent reflections	8040
R_{int}	0.0354
Final R_1 values ($I > 2\sigma(I)$)	0.0456
Final wR (F^2) values ($I > 2\sigma(I)$)	0.1367
Goodness of fit on F^2	1.046

Table S2 Gas sorption data for some best performing porous supramolecular organic framework materials.

	SA_{BET} ($m^2 \cdot g^{-1}$)	$V(N_2)$ ($mmol \cdot g^{-1}$)	$V(H_2)$ ($mmol \cdot g^{-1}$)	$V(CH_4)$ ($mmol \cdot g^{-1}$)				$V(CO_2)$ ($mmol \cdot g^{-1}$)			
		77 K	77 K	273 K	298 K	273 K	298 K	273 K	298 K	273 K	298 K
		1 bar	1 bar	1 bar	1 bar	20 bar	20 bar	1 bar	1 bar	20 bar	20 bar
SOF-7a	900[a]	2.9	0.03	0.29	0.22	2.11	1.71	2.85	1.49	7.07	5.48
HOF-8d[S12]	--	--	--	--	--	--	--	--	2.55	--	--
TTBI[S13]	2796[b]	34	10.8	0.94	--	--	--	3.61	--	--	--
SOF-1a[S1]	474[c]	6.4	--	--	--	1.43[e]	--	1.34	0.71	4.06[e]	3.08[e]
HOF-1a[S14]	359[d]	--	--	--	--	--	--	--	--	--	--
HOF-2a[S15]	238[d]	--	--	--	--	--	--	--	--	--	--
TBC[4]DHQ[S16]	230[b]	4.0	--	--	--	--	--	--	--	--	1.56[f]
TTP[S17]	--	--	--	--	0.38	--	--	--	0.98	--	--
CB[6][S18]	210	--	--	--	--	--	--	2.7(8)	2.2	--	3.4[g]
CB[7][S19]	293[d]	--	--	--	0.27[h]	--	--	2.8(7)	2.3[h]	--	--

[a] Calculated from CO_2 isotherm at 273 K; [b] determined by N_2 sorption at 77 K with data points in the range for P/P_0 between 0.01 and 0.04;
[c] Calculated from N_2 adsorption at 125 K and 1 bar; [d] determined by CO_2 adsorption at 196 K; [e] measured at 16 bar; [f] measured at 35 bar;
[g] measured at 30 bar; [h] measured at 297 K.

Table S3 Comparison of gas uptake of **SOF-7a** and **SOF-1a** for selectivity CO_2 over CH_4 at 16 bar.

Material	**CH_4 uptake at 1bar ($mmol \cdot g^{-1}$)**		**CH_4 uptake at 16 bar ($mmol \cdot g^{-1}$)**		**CH_4 uptake at 20 bar ($mmol \cdot g^{-1}$)**		**CO_2 uptake at 16 bar ($mmol \cdot g^{-1}$)**	**Selectivity CO_2 over CH_4**	
	273 K	298 K	273 K	298 K	273 K	298 K	298 K	273 K	298 K
SOF-7a	0.29	0.22		1.54	2.11	1.71	5.30	14.2	9.31
SOF-1a				1.43			3.08	5.60	4.24

Table S4 Summary of the binding energy and parameters for CO_2 binding in **SOF-7a**.

Dimer···CO_2	*Binding Energy with dispersion correction ($kj{\cdot}mol^{-1}$)*	*Binding Energy ($kj{\cdot}mol^{-1}$)*	*Interaction*	*Distance (Å)*	*Angle (°)*	*O=C=O Angle (°)*	*Charge Transfer (me)*
A	-35.19	-10.24	H-Bond N-H···O_1@CO_2	2.29 H···O_1@CO_2	165.22 N-H···O@ CO_2	178.17	+54.36
			Weak H-Bond C-H···O_1@CO_2	2.80 H···O_1@CO_2	140.59 C-H···O_1@CO_2		
			Weak H-Bond C-H···O_2@CO_2	2.79 H···O_2@CO_2	144.30 C-H···O_2@CO_2		
			CO···C@CO_2	2.83 O···C@CO_2	148.62 C-O···C@CO_2		
B	-29.75	-7.96	H-Bond N-H···O@CO_2	2.35 NH···O@CO_2	160.76 N-H···O@ CO_2	178.30	+22.72
			Weak H-Bond C-H···O@CO_2	2.79 H···O@CO_2	161.53 C-H···O@ CO_2		
			C-O···C@CO_2	2.79 O···C@CO_2	147.07 C-O··· C@CO_2		
C	-31.53	-10.90	H-Bond N_3-H···O@CO_2	2.30 H···O@CO_2	N_3-H···O@CO_2 152.12	178.83	-46.99
			C-N_1···C@CO_2	3.00 N_1···C@CO_2	148.45 C-N_1···C@CO_2		
			C-N_2···C@CO_2	3.00 N_2···C@CO_2	138.24 C-N_2···C@CO_2		
D	-18.87	-3.28	Weak H-Bond C-H···O_1@CO_2	2.68 H···O_1@CO_2	151.83 C-H···O_1@CO_2	177.60	+27.65
			Weak H-Bond C-H···O_2@CO_2	2.83 H···O_2@CO_2	154.91 C-H···O_2@CO_2		
			C-O···C@CO2	2.73 O···C@CO2	168.63 C-O···C@CO2		

Table S5 Tóth fitting parameters and Henry law constants for gas uptake in **SOF-7a**

Temperature	CH_4					CO_2				
	n_{sat}	b	t	R^2	K_H	n_{sat}	b	t	R^2	K_H
273K	3.573	0.089	0.979	0.9997	0.305	8.049	0.545	0.974	0.9993	4.317
298K	1.365	0.078	1.329	0.9998	0.201	8.247	0.256	0.907	0.9996	1.836

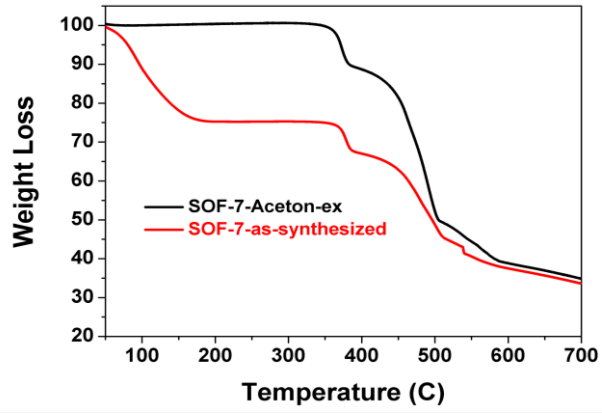

Figure S1 Thermogravimetric analysis (TGA) of the as-synthesized and acetone-exchanged samples of **SOF-7**. Samples were dried under N_2 flow upon loading before recording the TGA.

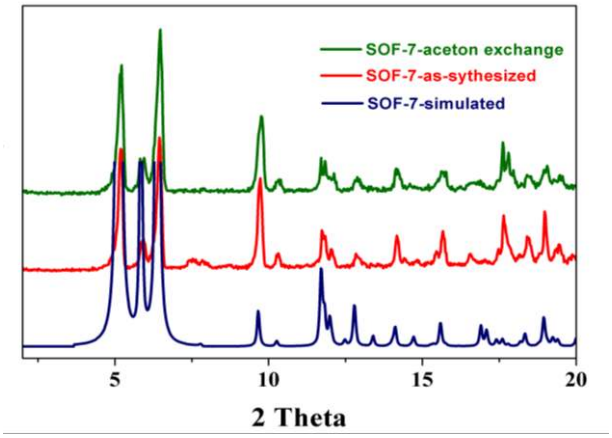

Figure S2 Powder X-ray diffraction (PXRD) of the simulated, as-synthesized and acetone-exchanged samples of **SOF-7**.

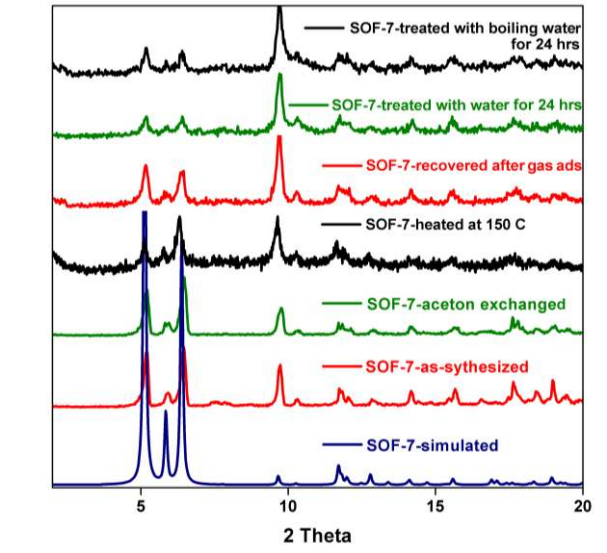

Figure S3 PXRD data for **SOF-7** under various conditions.

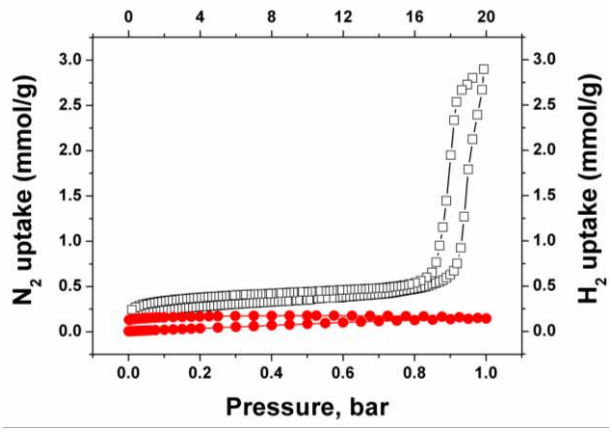

Figure S4 N_2 (black) and H_2 (red) uptake isotherms for **SOF-7a** at 77 K (black) in the pressure range 0 to 1bar (for N_2) and 0 to 20 bar (for H_2).

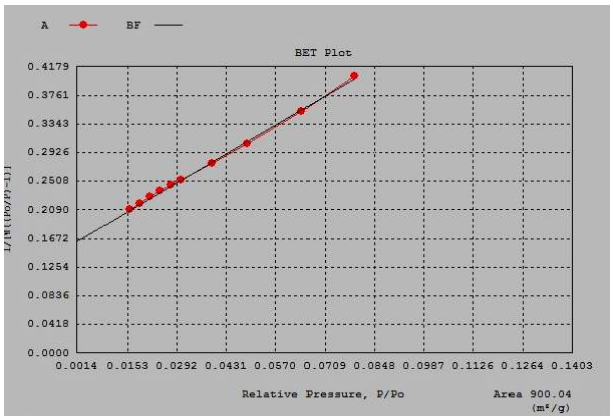

Figure S5 Brunauer-Emmett-Teller (BET) surface area of **SOF-7a** calculated from the CO_2 isotherm recorded at 273 K.

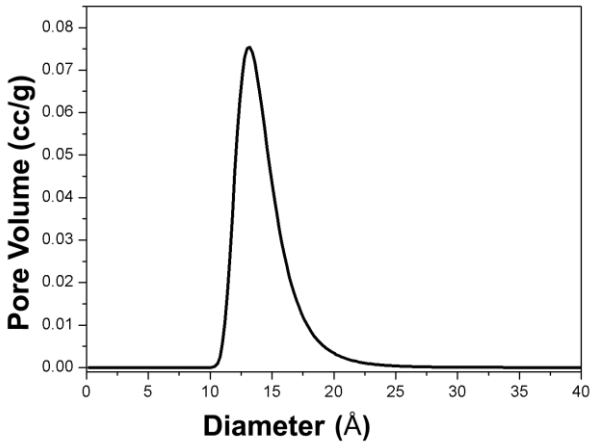

Figure S6 Pore size distribution (PSD) plot for **SOF-7a** calculated from the CO_2 adsorption isotherm at 273 K using Dubinin Asthakov (DA) methods.

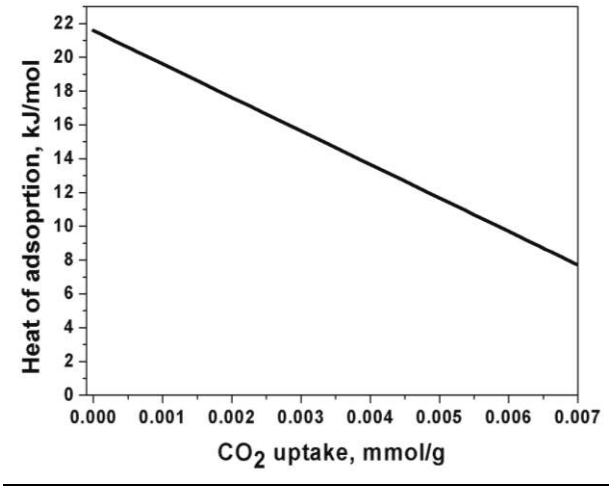

Figure S7 Heat of adsorption for **SOF-7a**.

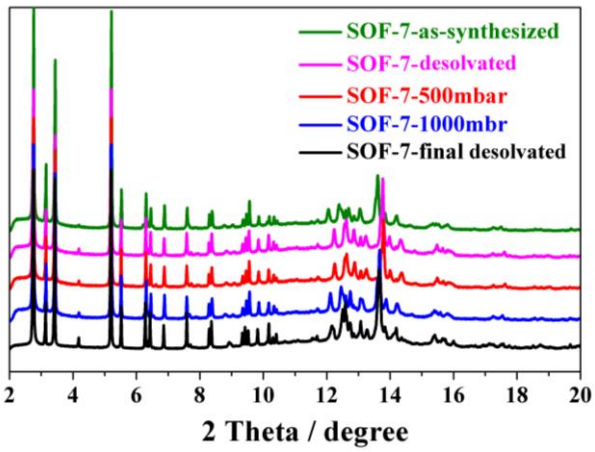

Figure S8 *In situ* PXRD patterns of CO_2 loaded **SOF-7a** in the pressure range 0 to 1 bar.

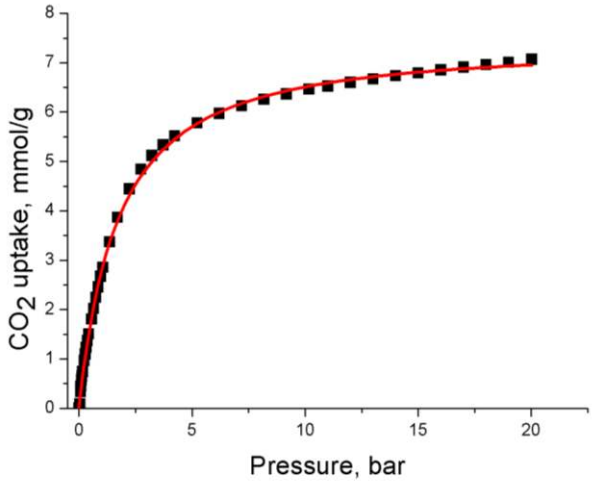

Figure S9 CO_2 isotherm at 273 K, black squares: experimental data fitted using Tóth model (red line).

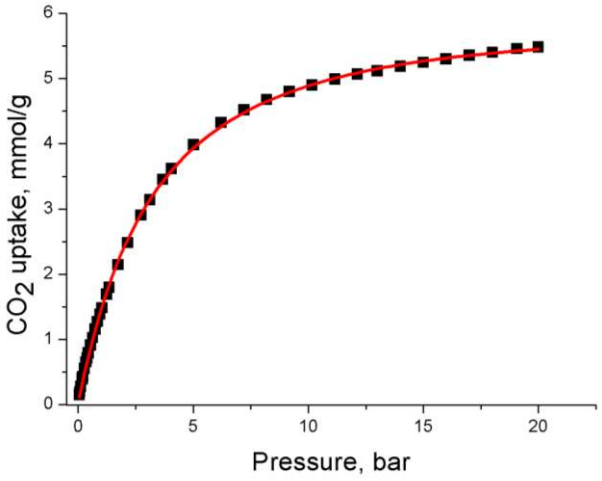

Figure S10 CO_2 isotherm at 298 K, black squares: experimental data fitted using Tóth model (red line).

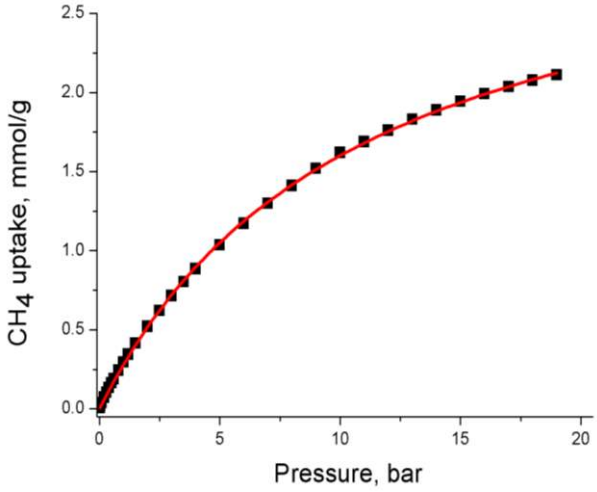

Figure S11 CH_4 isotherm at 273 K, black squares: experimental data fitted using Tóth model (red line).

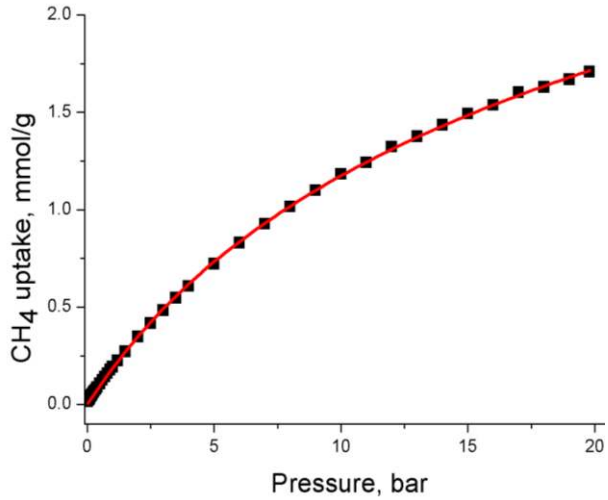

Figure S12 CH_4 isotherm at 298 K, black squares: experimental data fitted using Tóth model (red line).

References

[S1] (a) Yang, W.; Greenaway, A.; Lin, X.; Matsuda, R.; Blake, A. J.; Wilson, C.; Lewis, W.; Hubberstey, P.; Kitagawa, S.; Champness, N. R.; Schröder, M. *J. Am. Chem. Soc.* **2010**, *132*, 14457; (b) Ghozlan, S. A. S.; Hassanien, A. Z. A. *Tetrahedron* **2002**, *58*, 9423.

[S2] Alsmail, N. H.; Suyetin, M.; Yan, Y.; Cabot, R.; Krap, C. P.; Lü, J.; Easun, T. L.; Bichoutskaia, E.; Lewis, W.; A. Blake, J.; Schröder, M. *Chem. Eur. J.* **2014**, *20*, 7317.

[S3] Sheldrick, G. M. SHELXS97. *Acta Crystallogr., Sect. A* **2008**, *64*, 112.

[S4] Spek, A. L. *Acta Crystallogr., Sect. D* **2009**, *65*, 148.

[S5] Potoff, J. J.; Siepmann, J. I. *AIChE J.* **2002**, *47*, 1676.

[S6] Jorgensen, W. L.; Maxwell, D. S.; Tirado-Rives, J. *J. Am. Chem. Soc.* **1996**, *118*, 11225.

[S7] Yang, Q.; Zhong, C. *J. Phys. Chem. B* **2006**, *110*, 17776.

[S8] Peng, D.-Y.; Robinson, D. B. *Ind. Eng. Chem. Fundam.* **1976**, *15*, 59.

[S9] Shao, Y. et al. *Phys. Chem. Chem. Phys*., 2006, 8, 3172.

[S10] Gupta, A.; Chempath, S.; Sanborn, M. J.; Clark, L. A.; Snurr, R. Q. *Mol. Simul.* **2003**, *29*, 29.

[S11] Grimme, J.; Antony, S; Ehrlich, H.; Krieg, *J. Chem. Phys.* **2010**, *132*, 154104.

[S12] Luo, X.-Z.; Jia, X.-J.; Deng, J.-H.; Zhong, D.-C. *J. Am. Chem. Soc.* **2013**, *135*, 11684.

[S13] Mastalerz, M.; Oppel, I. M. *Angew. Chem. Int. Ed.* **2012**, *51*, 5252.

[S14] He, Y.; Xiang, S.; Chen, B. *J. Am. Chem. Soc.* **2011**, *133*, 14570.

[S15] Li, P.; He, Y.; Guang, J.; Weng, L.; Zhao, J. C.-G.; Xiang, S.; Chen, B. *J. Am. Chem. Soc.* **2014**, *136*, 547.

[S16] (a) Thallapally, P. K.; McGrail, B. P.; Atwood, J. L.; Gaeta, C.; Tedesco, C.; Neri, P. *Chem. Mater.* **2007**, *19*, 3355; (b) Msayib, K. J.; Book, D.; Budd, P. M.; Chaukura, N.; Harris, K. D. M.; Helliwell, M.; Tedds, S.; Walton, A.;Warren, J. E.; Xu, M.; McKeown, N. B. *Angew. Chem., Int. Ed.* **2009**, *48*, 3273.

[S17] (a) Sozzani, P.; Bracco, S.; Comotti, A.; Ferretti, L.; Simonutti, R. *Angew. Chem. Int. Ed.* **2005**,

44, 1816 ; (b) Couderc, G.; Hertzsch, T.; Behrnd, N.-R.; Krämer, K.; Hulliger, J. *Microporous Mesoporous Mater.* **2006**, *88*, 170.

[S18] Kim, H.; Kim, Y.; Yoon, M.; Lim, S.; Park, M. S.; Seo, G.; Kim, K. *J. Am. Chem. Soc.* **2010**, *132*, 12200.

[S19] Tian, J.; Ma, S.; Thallapally, P. K.; Fowler, D.; McGraila, B. P.; Atwood, J. L. *Chem. Commun.* **2011**, *47*, 7626.